The Response of UV/Blue Light and Ozone Sensing Using Ag-TiO₂ Planar Nanocomposite Thin Film

Tzu-Hsuan Lo [1], Pen-Yuan Shih [1] and Chiu-Hsien Wu [1,2,*]

[1]   Department of Physics, National Chung Hsing University, Taichung 402, Taiwan;
      a0970712400@gmail.com (T.-H.L.); a234851678@gmail.com (P.-Y.S.)
[2]   Institute of Nanoscience, National Chung Hsing University, Taichung 402, Taiwan
[*]   Correspondence: chwu@phys.nchu.edu.tw

Abstract: We successfully fabricated a planar nanocomposite film that uses a composite of silver nanoparticles and titanium dioxide film (Ag-TiO₂) for ultraviolet (UV) and blue light detection and application in ozone gas sensor. Ultraviolet-visible spectra revealed that silver nanoparticles have a strong surface plasmon resonance (SPR) effect. A strong redshift of the plasmonic peak when the silver nanoparticles covered the TiO₂ thin film was observed. The value of conductivity change for the Ag-TiO₂ composite is 4–8 times greater than that of TiO₂ film under UV and blue light irradiation. The Ag-TiO₂ nanocomposite film successfully sensed 100 ppb ozone. The gas response of the composite film increased by roughly six and four times under UV and blue light irradiation, respectively. We demonstrated that a Ag-TiO₂ composite gas sensor can be used with visible light (blue). The planar composite significantly enhances photo catalysis. The composite films have practical application potential for wearable devices.

Keywords: light sensor; SPR; composite; ppb-level ozone

1. Introduction

Due to growing environmental awareness, photocatalysts have been identified as green materials for reducing air pollution [1]. Titanium dioxide (TiO₂) is a popular photocatalytic material with considerable development potential [2,3]. With a bandgap of about 3.2 eV at an absorption wavelength of around 360 nm, TiO₂ is a widely-studied n-type metal-oxide semiconductor (MOS) that is commonly used in photocatalysts and gas sensors [4–6]. Enhancing light response is an important application of the light-harvesting and gas sensing capabilities of TiO₂. According to researchers, doping noble-metal particles can enhance the photocatalytic and degradation efficiency of TiO₂ for chemical or biological matter. Absorption spectra also show good response in visible light when TiO₂ nanocomposites (metal-doped TiO₂) are used [7–12]. Several methods, such as metal particle doping, polymer nanocomposites, and core-shell nanoparticles [13–16], have been developed to enhance photocatalysis. The primary reason for this enhancement is that the surface plasmon resonance (SPR) produced by these metal nanoparticles can significantly change the visible light response and electrical properties of semiconductors. Via the SPR effect, the metal-nanoparticle composite provides additional electrons to the semiconductor. Different metal nanoparticles (Ag, Au) doped on MOSs are widely used in many fields to generate SPR and enhance photocatalysis; they are also used in gas sensors, environmental protection technologies, solar cells, energy storage devices, and photoelectric materials [17–19]. For example, researchers have applied SPR with magnetic microspheres for prion protein detection [20–22], a magnetic biochip (Au/Fe₂O₃/Au) for antigen detection [23], core-shell γ-Fe2O3@Au nanoparticles for low-field nuclear magnetic resonance [24], a gold film-coated side-polished fiber for temperature sensor

fabrication [25], and Au@SiO$_2$ core-shell NPs into TiO$_2$ scaffold layer to increase the power conversion efficiency of solar cells [26].

With their excellent characteristics, MOSs doped with metal nanoparticles are highly desirable composite materials. In this study, we discuss the Ag-TiO$_2$ planar composite film [17]. The methods used in the complexation of metal nanoparticles in TiO$_2$ are primarily chemical-based. However, it is difficult to ensure the uniform doping of silver nanoparticles in TiO$_2$ for large-scale and mass production [18,19,27–29]. We coated silver nanoparticles with TiO$_2$ by electron-beam (e-beam) evaporation during the semiconductor fabrication process to ensure that the silver nanoparticles were in complete contact with the TiO$_2$, without the use of high-temperature annealing, while still successfully sensing 100 ppb ozone [17]. This approach can significantly improve the practical application of silver particles in areas such as the manufacturing of gas sensors and wearable devices. We discuss the electrical properties, light response, conductivity change, and gas sensing of the Ag-TiO$_2$ composite film for the detection of light and gas molecules.

2. Materials and Methods

We prepared the silver nanoparticles on a non-conductive glass and performed radio-frequency (RF)-magnetron sputtering at room temperature to deposit a silver film 10 nm thick. This film was then annealed at 250 °C for 1 h to produce nanoparticles. TiO$_2$ film was overlaid with silver nanoparticles. Using a Ti$_3$O$_5$ tablet as a starting material, we then performed e-beam evaporation at a working pressure of approximately 0.1 Torr to produce TiO$_2$ films with thicknesses of 10 nm, 20 nm, 30 nm, and 40 nm. The reaction equation is as follows [30,31]:

$$2Ti_3O_5 + O_2 \rightarrow 6TiO_2 \tag{1}$$

We labeled the Ag-TiO$_2$ films with thicknesses of 10 nm and 20 nm as AT10 and AT20, respectively. We labeled the TiO$_2$ films with thicknesses of 10 nm and 20 nm as T10 and T20, respectively. Using RF-magnetron sputtering, we deposited a gold film with a thickness of 100 nm on the sample as a measuring electrode. We used a multimeter (Keithley 2400) to measure the electrical properties. We determined the particle sizes, morphologies, and lattice structures of the silver nanoparticles by scanning electron microscopy (SEM) and X-ray spectroscopy, and measured the absorption spectra with a UV-Vis spectrometer.

In the experiments conducted to determine the light response and ozone detection, we used ultraviolet (UV) light and blue light-emitting diode as light sources. These measurements are described in detail elsewhere [32–34].

3. Results

3.1. Chacteristics of Ag-TiO$_2$

Figure 1 shows SEM images of the Ag nanoparticles and Ag-TiO$_2$ film [35]. In Figure 1a, we can see that the Ag nanoparticles are almost spherical in shape. The silver nanoparticles have a uniform distribution with ring-like aggregates. There are four main nanoparticle groups with diameters of 5 nm, 15 nm, 25 nm, and 35 nm, respectively, and a maximum size of about 70 nm, as shown in the inset of Figure 1a. The average size is about 28 ± 13.26 nm. There are few particles whose sizes are over 80 nm. Figure 1b shows the Ag nanoparticles covering the TiO$_2$ film; grains can be clearly observed on this Ag-TiO$_2$ composition film, with average sizes ranging from 50 nm to 80 nm. This indicates that the particle sizes increased after the deposition of the 20 nm thick TiO$_2$ film on the Ag nanoparticles. The image of the Ag-TiO$_2$ composite film also shows an uneven surface.

Figure 2 shows the X-ray diffraction pattern of the Ag-TiO$_2$ composite, in which we can see no distinct peak for the TiO$_2$ film. The small peak at 2θ = 38.08 can be indexed as (111) for the silver nanoparticles. TiO$_2$ films, without having undergone an annealing process by e-beam evaporation, are amorphous [3].
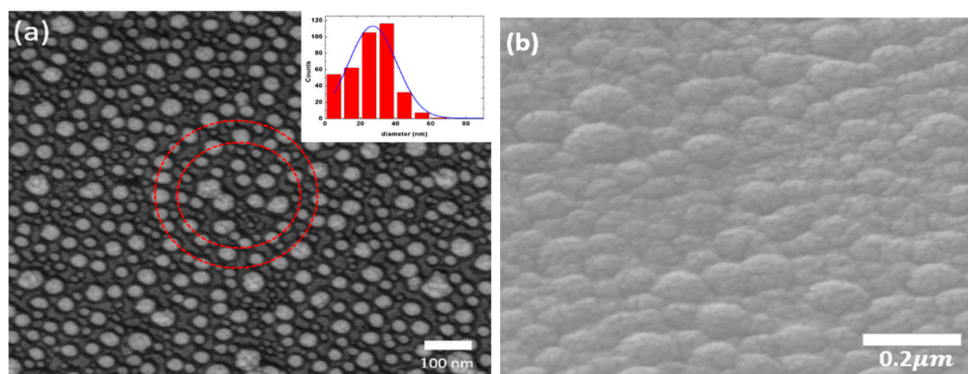
Figure 1. SEM images of the (**a**) Ag nanoparticles with the average size of 28 nm. The inset shows the distribution of particle sizes. (**b**) the Ag nanoparticles covering the TiO_2 film film.
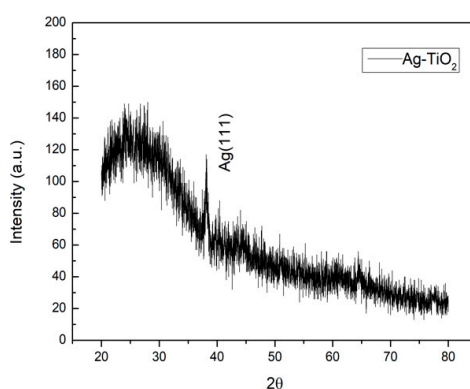

Figure 2. The X-ray diffraction pattern of the Ag-TiO_2 composite.

Figure 3a shows the transmittance and absorption spectra of the samples (Ag, T10, AT10, AT20, AT30, and AT40), as measured by a UV-Vis spectrometer. The absorption spectrum of the silver nanoparticles alone (without TiO_2 film) exhibits a clear and sharp peak at 429 nm, indicating silver spherical nanoparticles with the average sizes ranging from 30 to 50 nm [36,37]. This absorption spectrum indicates a localized SPR (LSPR) [38]. We can also see an unapparent peak at 360 nm in the absorption curve. The two resonance peaks in the UV-Vis spectra of the silver nanoparticles are mainly attributable to the dipole and multipole models (quadrupole) [39–41]. Multipole resonance is produced by a nonuniform electric field in the short-wavelength region, and it has been identified as hybrid quadrupole resonance. The main reason for the nonuniform polarization and electric fields is the nonlocal homogenized medium of the overlaid TiO_2 film or the nanoparticle distribution [42].
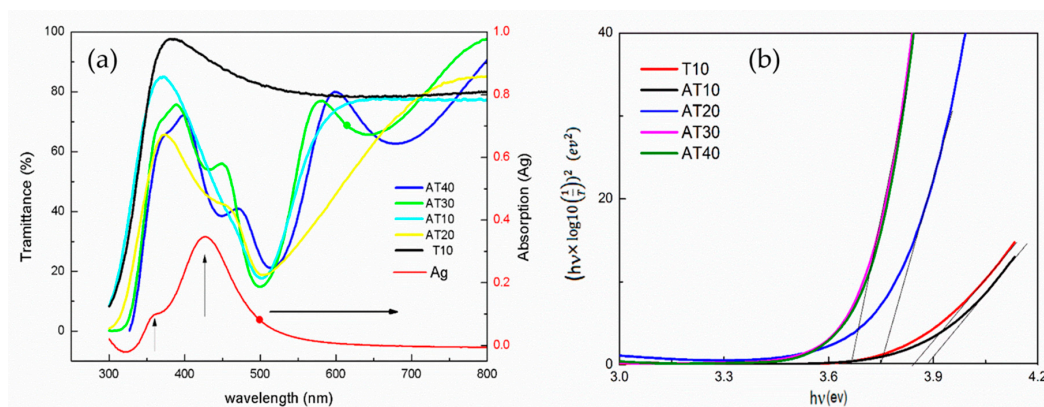

Figure 3. (**a**) The transmittance and absorption spectra of the samples. (**b**) The optical energy gap calculated by the Tauc equation.

The optical transmission spectra of T10 show that all of the TiO$_2$ films were highly transparent, i.e., more than 80%, in the visible region. Both the pure T10 and AT10 nanocomposites exhibit transmission edges at about 350 nm. The transmission spectra of AT10 and AT20 reveal a redshift due to the influence of the added silver nanoparticles. The spectra of AT10, AT20, AT30, and AT40 exhibit transmission edges at ~330 nm and a broad wave around 500 nm [17,19,20,29,30]. The transmission spectra of the semiconductor and metal nanoparticles overlap, which indicates that the TiO$_2$ and Ag metal nanoparticles were simultaneously excited by the light. There was also an edge at around 330 nm of the TiO$_2$ film and a peak at 500 nm due to the SPR of isolated silver nanoparticles in the samples. We found the resonance peak of the silver nanoparticles to be significantly affected by the TiO$_2$ film covering. The plasmon resonance of the silver nanoparticles was redshifted from a wavelength of 428 nm to 500 nm with TiO$_2$ films of 10–30 nm. As the thickness of the TiO$_2$ film increased to 40 nm, the redshift to 540 nm became more evident. The shift in the plasmon on this nanocomposite may be primarily attributable to the change in the permittivity of the medium. After coating, the oxide film has a much higher permittivity (ε_m). This variety of plasmonic peak can be briefly explained by the Drude model [43]:

$$W_{LSPR} \approx \frac{W_P}{\sqrt{1 + 2\varepsilon_m}} \tag{2}$$

where W_{LSPR} is the frequency of the LSPR, W_p is the plasma frequency of the bulky metal, and ε_m is the dielectric constant of the medium. However, the shift values of the experimental data and those calculated by the Drude model are slightly different. This difference may be due to the size, shape, and distribution of the silver nanoparticles.

The UV-Vis transmission spectra of the Ag-TiO$_2$ composites also reveal the transmittance to be less than 20%, which indicates that the composite films have a significant absorbance at the ~500-nm wavelength (blue light). The transmittance at wavelengths ranging from 300 to 600 nm is also less than 80%. This can be attributed to the fact that silver nanoparticles scatter the unabsorbed photons under light irradiation, resulting in an increase in the average photon path length, which increases the absorption [44]

Both the absorption peak of TiO$_2$ and the Ag resonance showed a redshift, which indicates a reduction in the optical bandgap energy. The optical energy gap (E_g) can be calculated using the Tauc equation:

$$(\alpha hv)^{\frac{1}{p}} = A(hv - E_g) \tag{3}$$

where A, E_g, h, and v are constant, energy gap, plank constant, and frequency, respectively; p is the characteristic value of the optical absorption process, which is equal to 2 because TiO$_2$ is an indirect energy gap material; and α is a coefficient. When the thickness of TiO$_2$ was increased from 10 nm to 40 nm, the bandgaps of T10, AT10, AT20, AT30, and AT40 were 3.84 3.88, 3.75, 3.66, and 3.66 eV, respectively. The band gaps shown in Figure 3b are smaller than that of the 10 nm TiO$_2$ film with increases in the thickness of the TiO$_2$. The bandgap reduced no further when the TiO$_2$ thickness was greater than the size of the Ag nanoparticles [45].

3.2. UV and Blue Light Response

Figure 4a,b show the resistance–time relationship (bias: 1 V) of the Ag-TiO$_2$ nanocomposite film (10 and 20 nm) and the TiO$_2$ film (10 and 20 nm) under UV irradiation. Electrons and holes are generated when the films are irradiated by UV light, and the increased number of free electrons reduces the resistance. The light response of the composite was more significant than that of the TiO$_2$ film, which means that the composite produced more electrons after UV irradiation [46].
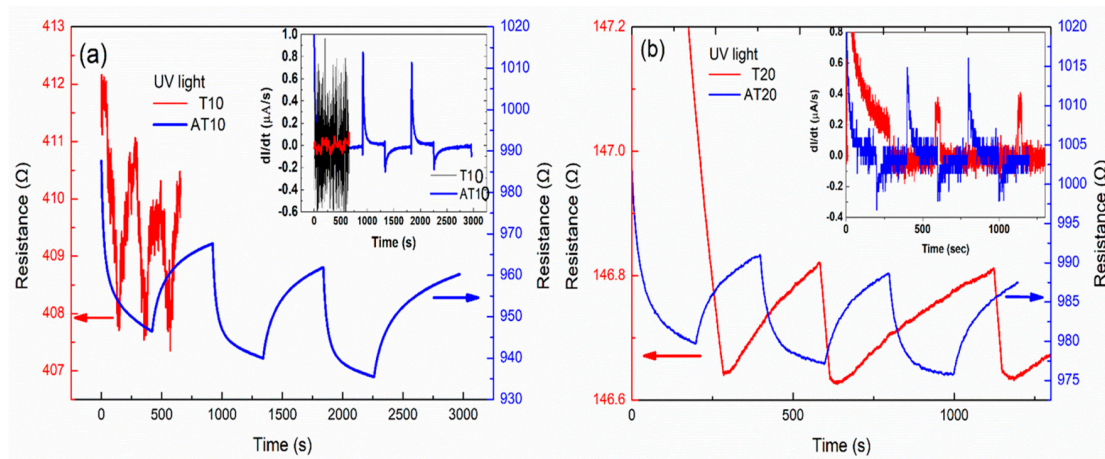
Figure 4. (**a**,**b**) show the resistance–time relation of Ag-TiO$_2$ and TiO$_2$ with different thickness under UV irradiation.

An increase in the electrical conductivity of TiO$_2$ under light irradiation and additional free carriers in the material can be generated in TiO$_2$. The relationship of the resistance of the samples with and without light irradiation is as follows:

$$R_L = R_d \left(\frac{\sigma_d}{\sigma_d + \Delta\sigma} \right), \; \frac{R_d}{R_L} = 1 + \frac{\Delta\sigma}{\sigma_d}, \tag{4}$$

where R_L, R_d, σ_d, and $\Delta\sigma$ are the resistance with light irradiation, resistance in the dark, the conductivity, and the conductivity change, respectively. According to the above equation, the percentages of $\Delta\sigma/\Delta\sigma_d$ for T10, T20, AT10, and AT20 for 50 s of light irradiation are 0.4%, 0.13%, 1.9%, and 1.1%, respectively. The value of $\Delta\sigma/\Delta\sigma_d$ for Ag-TiO$_2$ is 4–8 times greater than that of TiO$_2$, which means that the conductivity of the semiconductors was obviously improved by doping them with metal nanoparticles. The conductivity increase indicates that either the carrier density or carrier mobility increased.

The insets of Figure 4a,b show the relationship between the rate of photocurrent change and the detection time. The current density is given by J = σE. The conductivity is $\sigma_0 = n_0 e\mu_0$, where n_0 and μ_0 are the carrier density and mobility in the dark, respectively. The conductivity (σ_L) in light will increase to $\sigma_L = \sigma_0 + \Delta\sigma$. The current change rate is given by dI/dt $\propto$ dσ/dt $\propto$ Δσ/Δt and is proportional to the carrier conductivity rate, where $\Delta\sigma$ is attributed to the change in carrier density (Δn) and carrier mobility ($\Delta\mu$). The resistance curves of AT10 and AT20 are more stable and significant than those of T10 and T20 (bias: 1 volt). The maximum current change rates of AT10 and AT20 are 0.7–0.8 and 0.4–0.5 (A/s), respectively, and are more significant than those of T10 and T20. The change is small for TiO$_2$ under the same UV intensity. The differential curve fluctuated widely and was smoothed and averaged by several points. This variation is due to the SPR of the silver nanoparticles, whereby the silver nanoparticles provide TiO$_2$ with hot electrons and reduce its optical band gap, thus generating more electrons in the conduction band of TiO$_2$ with UV light irradiation.

The light response (($I_L - I_d$)/I_d) of light for 50 s irradiation is shown in Table 1. Therefore, the photo response of the Ag-TiO$_2$ composite is better than that of the TiO$_2$ film. This reveals that the generation and recombination rates of electrons and holes in the Ag-TiO$_2$ composite film are much greater and faster than those of the TiO$_2$ film [46].

Table 1. The response (($I_L - I_d$)/I_d) of light for 50 s light irradiation.

	T10	AT10	T20	AT20
UV	0.2%	1.7%	0.1%	1.2%
Blue	X	0.45%	X	0.46%

When the Ag-TiO$_2$ composite film is irradiated by blue light, the silver nanoparticles absorb the blue light to produce hot electrons for TiO$_2$ and reduce the resistance value (Figure 5). This means that the composite film can absorb blue light. However, the 10 nm and 20 nm-thick TiO$_2$ films showed no response to blue light.
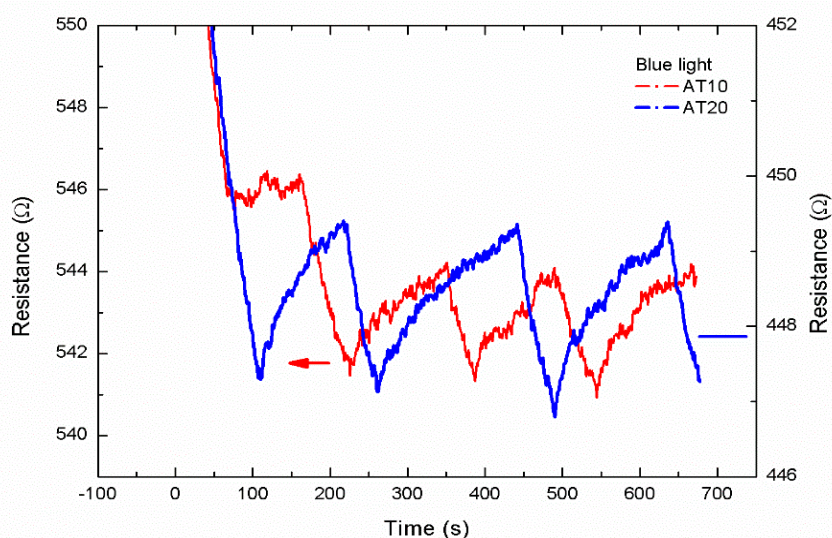

Figure 5. Ag-TiO$_2$ composite film is irradiated by blue light.

3.3. Gas Sensing

Ozone is known to be an oxidizing gas. Figure 6 shows the resistance–time relationship of films at an ozone concentration of 100 ppb, which is the index value indicating damage to human health. TiO$_2$ is an n-type semiconductor, and we generated more electrons and holes by light irradiation [47,48]. The ozone concentration of the test box is simultaneously measured by a commercial ozone monitor (2B Tech 106-L) [32,33]. When strongly oxidizing O$_3$ was introduced (25 °C and relative humidity ~45 ± 3%), adsorption and desorption reactions occurred simultaneously. Since an oxidizing gas was adsorbed on the TiO$_2$, the free electrons were trapped, causing a decrease in the number of free electrons and an increase in resistance. In our experiment, UV and blue light were used to excite electrons, and thereby, facilitate gas absorption by the films. In Figure 6a, we can see a noticeable change in the resistance upon the introduction of ozone to the test chamber. There was little difference in the resistance changes of films under different types of light irradiation. Figure 6b shows the dR/dt versus time relationship of films under different types of light. The resistance changes of T20 (UV), AT20 (UV), and AT20 (blue) were 0.005, 0.03, and 0.02, respectively, at 100 ppb of ozone. Thus, the composite film AT20 exhibited a better response than the TiO$_2$ film. The sensitivities of ozone for 300 s exposure are shown in Table 2. The sensitivity, i.e., AT20 (UV) > AT20 (Blue) > T20 (UV) >> AT20, revealed the good performance of the composite film with respect to ozone. The response of the composite film increased by roughly six and four times under UV and blue light irradiation, respectively. The silver nanoparticles enhanced the effectiveness of the transfer of free electrons from the conduction band of TiO$_2$ to ozone. Thus, we demonstrated that the Ag-TiO$_2$ composite gas sensor can be used with visible light. In Table 3, we summarize the sensitivities for ozone using different materials, as obtained by various research groups.
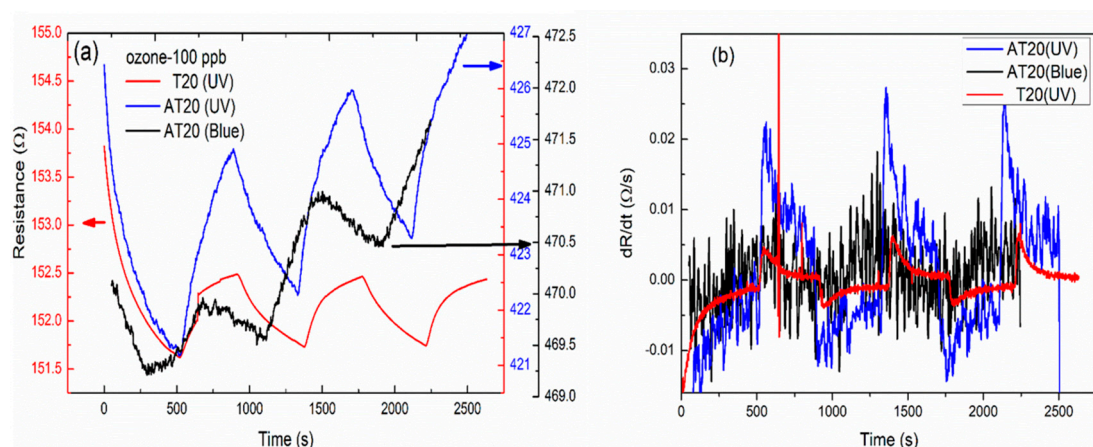
Figure 6. (**a**) The resistance–time relation of films at an ozone concentration of 100 ppb under different light irradiation. (**b**) Differential curves under light irradiation.

Table 2. The sensitivity (($R_g - R_a)/R_a$) of gas ozone for 300 s gas exposure.

	T20		AT20	
	Blue	**UV**	**Blue**	**UV**
Ozone	X	0.35%	0.38%	0.8%

Table 3. The response of ozone using different materials (R. T: Room temperature, * S = R_g/R_{air}, # S = (R_g − Rair)/Rair).

Materials	Ozone (ppb)	Operating Temperature	Response	Reference
core–shell Au@TiO$_2$	500	R. T	1.15 *	[16]
V$_2$O$_5$/TiO$_2$	1000	300 °C	1.4 #	[49]
Zn$_{0.95}$Co$_{0.05}$O	20	250 °C	0.4 #	[50]
CuWO$_4$	15	250 °C	~2 *	[51]
Pt/TiO$_2$-SnO$_2$	2500	R.T.(UV)	1100 *	[52]
Ag/TiO$_2$	100	R.T. (Blue)	1.004 *	Present study

4. Conclusions

In this study, we successfully used a composite of silver nanoparticles and titanium dioxide film (Ag-TiO$_2$). Ultraviolet-visible spectra revealed that silver nanoparticles have a strong SPR effect. In addition, we observed a strong redshift of the plasmonic peak when the silver nanoparticles covered the TiO$_2$ thin film.

When measuring the light and gas responses, we found the light response of the composite film to be more versatile and responsive due to the SPR effect with UV irradiation. Under UV and blue light irradiation, the silver-nanoparticle electrons become excited and supplement those of the TiO$_2$ film. The value of conductivity change for Ag-TiO$_2$ is 4–8 times greater than that of TiO$_2$ under light irradiation. We determined that the SPR effect provides additional electrons to the TiO$_2$, thereby improving the light response and sensitivity of the gas sensor. We also found the conductivity of TiO$_2$ to increase with Ag doping. In our experiments, the Ag-TiO$_2$ nanocomposite film successfully sensed 100 ppb ozone. The gas sensor can also be operated with blue light; the results showed that the composite film could absorb blue light, and thus, can be used for application in different sensors such as gas sensors, light sensors, biosensors, and smart windows [53].

Author Contributions: C.-H.W. conceived and designed the experiments, and wrote the manuscript; T.-H.L. and P.-Y.S. performed the experiments.

Conflicts of Interest: The authors declare no conflict of interest.

References

1. Li, X.; Xie, J.; Jiang, C.; Yu, J.; Zhang, P. Review on design and evaluation of environmental photocatalysts. *Front. Environ. Sci. Eng.* **2018**, *12*, 14. [CrossRef]
2. Anpo, M.; Kamat, P.V. *Environmentally Benign Photocatalysts: Applications of Titanium Oxide-Based Materials*; Springer: New York, NY, USA, 2010.
3. Schneider, J.; Matsuoka, M.; Takeuchi, M.; Zhang, J.; Horiuchi, Y.; Anpo, M.; Bahnemann, D.W. Understanding TiO_2 Photocatalysis: Mechanisms and Materials. *Chem. Rev.* **2014**, *114*, 9919–9986. [CrossRef] [PubMed]
4. Kumar, S.G.; Devi, L.G. Review on Modified TiO_2 Photocatalysis under UV/Visible Light: Selected Results and Related Mechanisms on Interfacial Charge Carrier Transfer Dynamics. *J. Phys. Chem. A* **2011**, *115*, 13211–13241. [CrossRef] [PubMed]
5. Shehzad, N.; Tahir, M.; Johari, K.; Murugesan, T.; Hussain, M. A critical review on TiO_2 based photocatalytic CO_2 reduction system: Strategies to improve efficiency. *J. CO_2 Util.* **2018**, *26*, 98–122. [CrossRef]
6. Pelaez, M.; Nolan, N.T.; Pillai, S.C.; Seery, M.K.; Falaras, P.; Kontos, A.G.; Dunlop, P.S.; Hamilton, J.W.; Byrne, J.A.; O'shea, K.; et al. A review on the visible light active titanium dioxide photocatalysts for environmental applications. *Appl. Catal. B Environ.* **2012**, *125*, 331–349. [CrossRef]
7. Ayati, A.; Ahmadpour, A.; Bamoharram, F.F.; Tanhaei, B.; Mänttäri, M.; Sillanpää, M. A review on catalytic applications of Au/TiO2 nanoparticles in the removal of water pollutant. *Chemosphere* **2014**, *107*, 163–174. [CrossRef]
8. Maijenburg, A.W.; Veerbeek, J.; de Putter, R.; Veldhuis, S.A.; Zoontjes, M.G.; Mul, G.; Montero-Moreno, J.M.; Nielsch, K.; Schäfer, H.; Steinhart, M.; et al. Electrochemical synthesis of coaxial TiO_2-Ag nanowires and their application in photocatalytic water splitting. *J. Mater. Chem. A* **2014**, *2*, 2648–2656. [CrossRef]
9. Zieli´nska-Jurek, A.; Zaleska, A. Ag/Pt-modified TiO_2 nanoparticles for toluene photooxidation in the gas phase. *Catal. Today* **2014**, *230*, 104–111. [CrossRef]
10. He, C.; Xiong, Y.; Chen, J.; Zha, C.; Zhu, X. Photoelectrochemical performance of Ag-TiO_2/ITO film and photoelectrocatalytic activity towards the oxidation of organic pollutants. *J. Photochem. Photobiol. A Chem.* **2013**, *157*, 71–79. [CrossRef]
11. Yu, D.H.; Yu, X.; Wang, C.; Liu, X.C.; Xing, Y. Synthesis of natural cellulose-templated TiO_2/Ag nanosponge composites and photocatalytic properties. *ACS Appl. Mater. Interfaces* **2012**, *4*, 2781–2787. [CrossRef]
12. Ge, M.Z.; Cao, C.Y.; Li, S.H.; Tang, Y.X.; Wang, L.N.; Qi, N.; Huang, J.Y.; Zhang, K.Q.; Al-Deyab, S.S.; Lai, Y.K. In situ plasmonic Ag nanoparticle anchored TiO_2 nanotube arrays as visible-light-driven photocatalysts for enhanced water splitting. *Nanoscale* **2016**, *8*, 5226–5234. [CrossRef] [PubMed]
13. Kim, J.H.; Mirzaei, A.; Kim, H.W.; Kim, S.S. Extremely sensitive and selective sub-ppm CO detection by the synergistic effect of Au nanoparticles and core–shell nanowires. *Sens. Actuators B Chem.* **2017**, *249*, 177–188. [CrossRef]
14. Genix, A.C.; Schmitt-Pauly, C.; Alauzun, J.G.; Bizien, T.; Mutin, P.H.; Oberdisse, J. Tuning Local Nanoparticle Arrangements in TiO_2-Polymer Nanocomposites by Grafting of Phosphonic Acids. *Macromolecules* **2017**, *50*, 7721–7729. [CrossRef]
15. Hirakawa, T.; Kamat, P.V. Charge separation and catalytic activity of Ag@TiO_2–core-shell composite clusters under UV-irradiation. *J. Am. Chem. Soc.* **2005**, *127*, 3928–3934. [CrossRef] [PubMed]
16. Zhu, Z.; Chang, J.L.; Wu, R.J. Fast ozone detection by using a core–shell Au@TiO_2 sensor at room temperature. *Sens. Actuators B Chem.* **2015**, *214*, 56–62. [CrossRef]
17. Singh, J.; Sahu, K. Thermal annealing induced strong photoluminescence enhancement in Ag-TiO2 plasmonic nanocomposite thin films. *J. Alloys Compd.* **2019**, *786*, 750–757. [CrossRef]
18. Shao, X.; Li, B.; Zhang, B.; Shao, L.; Wu, Y. Au@ZnO core–shell nanostructures with plasmon-induced visible-light photocatalytic and photoelectrochemical properties. *Inorg. Chem. Front.* **2016**, *3*, 934–943. [CrossRef]
19. Wu, W.Y.; Hsu, C.F.; Wu, M.J.; Chen, C.N.; Huang, J.J. Ag–TiO_2 composite photoelectrode for dye-sensitized solar cell. *Appl. Phys. A* **2017**, *123*, 357. [CrossRef]

20. Lou, Z.; Han, H.; Zhou, M.; Wan, J.; Sun, Q.; Zhou, X.; Gu, N. Fabrication of Magnetic Conjugation Clusters via Intermolecular Assembling for Ultrasensitive Surface Plasmon Resonance (SPR) Detection in a Wide Range of Concentrations. *Anal. Chem.* **2017**, *89*, 13472–13479. [CrossRef]

21. Lou, Z.; Han, H.; Mao, D.; Jiang, Y.; Song, J. Qualitative and Quantitative Detection of PrP^{Sc} Based on the Controlled Release Property of Magnetic Microspheres Using Surface Plasmon Resonance (SPR). *Nanomaterials* **2018**, *8*, 107. [CrossRef]

22. Lou, Z.; Wan, J.; Zhang, X.; Zhang, H.; Zhou, X.; Cheng, S.; Gu, N. Quick and sensitive SPR detection of prion disease-associated isoform(PrPSc) based on its self-assembling behavior on bare gold film andspecific interactions with aptamer-graphene oxide (AGO). *Colloids Surf. B Biointerfaces* **2017**, *157*, 31–39. [CrossRef] [PubMed]

23. Deng, Z.Y.; Chen, K.L.; Wu, C.H. Improving the SERS signals of biomolecules using a stacked biochip containing Fe$_2$O$_3$/Au nanoparticles and a DC magnetic field. *Sci. Rep.* **2019**, *9*, 9566. [CrossRef] [PubMed]

24. Chen, K.L.; Yeh, Y.W.; Chen, J.M.; Hong, Y.J.; Huang, T.L.; Deng, Z.Y.; Wu, C.H.; Liao, S.H.; Wang, L.M. Influence of magnetoplasmonic γ-Fe$_2$O$_3$/Au core/shell nanoparticles on low-field nuclear magnetic resonance. *Sci. Rep.* **2016**, *6*, 35477. [CrossRef] [PubMed]

25. Liu, S.; Cao, S.; Zhang, Z.; Wang, Y.; Liao, C.; Wang, Y. Temperature Sensor Based on Side-Polished Fiber SPR Device Coated with Polymer. *Sensors* **2019**, *19*, 4063. [CrossRef]

26. Qi, F.; Wang, C.; Cheng, N.; Liu, P.; Xiao, Y.; Li, F.; Sun, X.; Liu, W.; Guo, S.; Zhao, X.Z. Improving the performance through SPR effect by employing Au@SiO$_2$ core-shell nanoparticles incorporated TiO$_2$ scaffold in efficient hole transport material free perovskite solar cells. *Electrochim. Acta* **2018**, *282*, 10–15. [CrossRef]

27. Sun, S.-Q.; Sun, B.; Zhang, W.; Wang, D. Preparation and antibacterial activity of Ag-TiO$_2$ composite film by liquid phase deposition (LPD) method. *Bull. Mater. Sci.* **2008**, *31*, 61–66. [CrossRef]

28. Wang, H.; Faria, J.L.; Dong, S.; Chang, Y. Mesoporous Au/TiO$_2$ composites preparation, characterization, and photocatalytic properties. *Mater. Sci. Eng. B* **2012**, *177*, 913–919. [CrossRef]

29. Binyu, Y.; Man, L.K.; Qiuquan, G.; Ming, L.W.; Jun, Y. Synthesis of Ag-TiO$_2$ composite nano thin film for antimicrobial application. *Nanotechnology* **2011**, *22*, 115603.

30. Wang, F.X.; Hwangbo, C.K.; Jung, B.Y.; Lee, J.H.; Park, B.H.; Kim, N.Y. optical and structural properties of TiO2 films deposited from Ti$_3$O$_5$ by electron beam. *Surf. Coat. Technol.* **2007**, *201*, 5367–5370. [CrossRef]

31. Shei, S.-C. Optical and Structural Properties of Titanium Dioxide Films from TiO$_2$ and Ti$_3$O$_5$ Starting Materials Annealed at Various Temperatures. *Adv. Mater. Sci. Eng.* **2013**, *2013*, 545076. [CrossRef]

32. Lin, C.W.; Huang, K.L.; Chang, K.W.; Chen, J.H.; Chen, K.L.; Wu, C.H. Ultraviolet photodetector and gas sensor based on amorphous In-Ga-Zn-O film. *Thin Solid Film.* **2016**, *618*, 73–76. [CrossRef]

33. Wu, C.H.; Jiang, G.J.; Chiu, C.C.; Paul, C.; Jeng, C.C.; Wu, R.J.; Chen, J.H. Fast gas concentration sensing by analyzing the rate of resistance change. *Sens. Actuators B* **2015**, *209*, 906–910. [CrossRef]

34. Wu, C.H.; Chang, K.W.; Li, Y.N.; Deng, Z.Y.; Chen, K.L.; Jeng, C.C.; Wu, R.J.; Chen, J.H. Improving the sensitive and selective of trace amount ozone sensor on Indium-Gallium-Zinc Oxide thin film by ultraviolet irradiation. *Sens. Actuators B* **2018**, *273*, 1713–1718. [CrossRef]

35. Liu, X.; Li, D.; Sun, X.; Li, Z.; Song, H.; Jiang, H.; Chen, Y. Tunable Dipole Surface Plasmon Resonances of Silver Nanoparticles by Cladding Dielectric Layers. *Sci. Rep.* **2015**, *5*, 12555. [CrossRef]

36. Lee, K.C.; Lin, S.J.; Lin, C.H.; Tsai, C.S.; Lu, Y.J. Size effect of Ag nanoparticles on surface plasmon resonance. *Surf. Coat. Technol.* **2008**, *202*, 5339–5342. [CrossRef]

37. Lee, S.Y.; Cho, E.S.; Kwon, S.J. The optical analyses of the multilayer transparent electrode and the formation of ITO/Mesh-Ag/ITO multilayers for enhancing an optical transmittance. *Appl. Surf. Sci.* **2019**, *487*, 990–999. [CrossRef]

38. Sanzone, G.; Zimbone, M.; Cacciato, G.; Ruffino, F.; Carles, R.; Privitera, V.; Grimaldi, M.G. Ag/TiO$_2$ nanocomposite for visible light-driven photocatalysis. *Superlattices Microstruct.* **2018**, *123*, 394–402. [CrossRef]

39. Jiang, M.M.; Chen, Y.H.; Li, H.B.; Liu, W.K.; Shan, X.C.; Shen, Z.D. Hybrid quadrupolar resonances stimulated at short wavelengths using coupled plasmonic silver nanoparticle aggregation Hybrid quadrupolar resonances stimulated at short wavelengths using coupled plasmonic silver nanoparticle aggregation. *J. Mater. Chem. C* **2014**, *2*, 56–63. [CrossRef]

40. Hooshmand, N.; Mostafa, A. El-Sayed, Collective multipole oscillations direct the plasmonic coupling at the nanojunction interfaces. *Proc. Natl. Acad. Sci. USA* **2019**, *116*, 19299–19304. [CrossRef]

41. Miroshnichenko, A.E.; Kivshar, Y.S. Fano Resonances in All-Dielectric Oligomers. *Nano Lett.* **2012**, *12*, 6459–6463. [CrossRef]

42. Yakovlev, A.B.; Hedayati, M.; Silveirinha, M.G.; Hanson, G.W. Local thickness-dependent permittivity model for nonlocal bounded wire-medium structures. *Phys. Rev. B* **2016**, *94*, 155442. [CrossRef]

43. Zhang, X.; Chen, Y.L.; Liu, R.S.; Tsai, D.P. Plasmonic photocatalysis. *Rep. Prog. Phys.* **2013**, *76*, 046401. [CrossRef] [PubMed]

44. Méndez-Medrano, M.G.; Kowalska, E.; Lehoux, A.; Herissan, A.; Ohtani, B.; Bahena, D.; Briois, V.; Colbeau-Justin, C.; Rodríguez-López, J.L.; Remita, H. Surface Modification of TiO_2 with Ag Nanoparticles and CuO Nanoclusters for Application in Photocatalysis. *J. Phys. Chem. C* **2016**, *120*, 5143–5154. [CrossRef]

45. Khore, S.K.; Kadam, S.R.; Naik, S.D.; Kale, B.B.; Sonawane, R.S. Solar light active plasmonic Au@TiO_2 nanocomposite with superior photocatalytic performance for H_2 production and pollutant degradation. *New J. Chem.* **2018**, *42*, 10958–10968. [CrossRef]

46. Sharma, A.; Kumar, R.; Bhattacharyya, B.; Husale, S. Hot electron induced NIR detection in CdS films. *Sci. Rep.* **2016**, *6*, 22939. [CrossRef] [PubMed]

47. Buso, D.; Post, M.; Cantalini, C.; Mulvaney, P.; Martucci, A. Gold Nanoparticle-Doped TiO_2 Semiconductor Thin Films: Gas Sensing Properties. *Adv. Funct. Mater.* **2008**, *18*, 3843–3849. [CrossRef]

48. Rai, P.; Khan, R.; Raj, S.; Majhi, S.M.; Park, K.K.; Yu, Y.T.; Lee, I.H.; Sekhar, P.K. Au@Cu_2O core–shell nanoparticles as chemiresistors for gas sensor applications: Effect of potential barrier modulation on the sensing performance. *Nanoscale* **2014**, *6*, 581–588. [CrossRef]

49. Avansi, W., Jr.; Catto, A.C.; da Silva, L.F.; Fiorido, T.; Bernardini, S.; Mastelaro, V.R.; Aguir, K.; Arenal, R. One-Dimensional V_2O_5/TiO_2 Heterostructures for Chemiresistive Ozone Sensors. *ACS Appl. Nano Mater.* **2019**, *2*, 4756–4764. [CrossRef]

50. Onofre, Y.J.; Catto, A.C.; Bernardini, S.; Fiorido, T.; Aguir, K.; Longo, E.; Mastelaro, V.R.; da Silva, L.F.; de Godoy, M.P. Highly selective ozone gas sensor based on nanocrystalline $Zn_{0.95}Co_{0.05}O$ thin film obtained via spray pyrolysis technique. *Appl. Surf. Sci.* **2019**, *478*, 347–354. [CrossRef]

51. Catto, A.C.; Fiorido, T.; Souza, É.L.; Avansi, W., Jr.; Andres, J.; Aguir, K.; Longo, E.; Cavalcante, L.S.; Da Silva, L.F. Improving the ozone gas-sensing properties of $CuWO_4$ nanoparticles. *J. Alloys Compd.* **2018**, *748*, 411–417. [CrossRef]

52. Wu, R.J.; Chen, C.Y.; Chen, M.H.; Sun, Y.L. Photoreduction measurement of ozone using Pt/TiO_2–SnO_2 material at room temperature. *Sens. Actuators B Chem.* **2007**, *123*, 1077–1082. [CrossRef]

53. Nunes, D.; Pimentel, A.; Gonçalves, A.; Pereira, S.; Branquinho, R.; Barquinha, P.; Fortunato, E.; Martins, R. Metal oxide nanostructures for sensor applications. *Semicond. Sci. Technol.* **2019**, *34*, 043001. [CrossRef]